Immunity
Article

The Pseudokinase MLKL Mediates Necroptosis via a Molecular Switch Mechanism

James M. Murphy,[1,2,6,*] Peter E. Czabotar,[1,2,6] Joanne M. Hildebrand,[1,2,6] Isabelle S. Lucet,[3] Jian-Guo Zhang,[1,2] Silvia Alvarez-Diaz,[1,2] Rowena Lewis,[1,2] Najoua Lalaoui,[1,2] Donald Metcalf,[1,2] Andrew I. Webb,[1,2] Samuel N. Young,[1,2] Leila N. Varghese,[1,2] Gillian M. Tannahill,[1,2] Esme C. Hatchell,[1,2] Ian J. Majewski,[1,2] Toru Okamoto,[1,2] Renwick C.J. Dobson,[4,5] Douglas J. Hilton,[1,2] Jeffrey J. Babon,[1,2] Nicos A. Nicola,[1,2] Andreas Strasser,[1,2] John Silke,[1,2] and Warren S. Alexander[1,2]

[1]The Walter and Eliza Hall Institute of Medical Research, Parkville, VIC 3052, Australia
[2]Department of Medical Biology, University of Melbourne, Parkville, VIC 3050, Australia
[3]Department of Biochemistry and Molecular Biology, School of Biomedical Sciences, Monash University, Clayton, VIC 3800, Australia
[4]Biomolecular Interactions Centre, School of Biological Sciences, University of Canterbury, Christchurch 8140, New Zealand
[5]Department of Biochemistry and Molecular Biology, University of Melbourne, Parkville, VIC 3010, Australia
[6]These authors contributed equally to this work
*Correspondence: jamesm@wehi.edu.au
http://dx.doi.org/10.1016/j.immuni.2013.06.018

SUMMARY

Mixed lineage kinase domain-like (MLKL) is a component of the "necrosome," the multiprotein complex that triggers tumor necrosis factor (TNF)-induced cell death by necroptosis. To define the specific role and molecular mechanism of MLKL action, we generated MLKL-deficient mice and solved the crystal structure of MLKL. Although MLKL-deficient mice were viable and displayed no hematopoietic anomalies or other obvious pathology, cells derived from these animals were resistant to TNF-induced necroptosis unless MLKL expression was restored. Structurally, MLKL comprises a four-helical bundle tethered to the pseudokinase domain, which contains an unusual pseudoactive site. Although the pseudokinase domain binds ATP, it is catalytically inactive and its essential nonenzymatic role in necroptotic signaling is induced by receptor-interacting serine-threonine kinase 3 (RIPK3)-mediated phosphorylation. Structure-guided mutation of the MLKL pseudoactive site resulted in constitutive, RIPK3-independent necroptosis, demonstrating that modification of MLKL is essential for propagation of the necroptosis pathway downstream of RIPK3.

INTRODUCTION

Caspases, activated on oligomeric platforms or by proteolytic cleavage, are the effector molecules of apoptosis, cleaving hundreds of cellular proteins, thereby resulting in cellular dismantling and characteristic apoptotic morphology. In contrast, programmed necrosis, or necroptosis, occurs when apoptosis and caspase activity are inhibited and is thought to provide an important defense against intracellular pathogens that can suppress classical apoptotic cell death (Vandenabeele et al., 2010; Vanlangenakker et al., 2012). Cytotoxic stimuli, such as tumor necrosis factor receptor 1 (TNFR1) ligation, trigger the assembly of intracellular complexes that activate prosurvival and inflammatory NF-κB and MAPK signaling pathways (Wertz and Dixit, 2010), but they can also activate caspase-8. In most situations prosurvival signaling from TNFR1, in particular NF-κB-mediated transcriptional upregulation of the caspase-8 inhibitor cFLIP, inhibits apoptosis (Micheau et al., 2001). However, when NF-κB is inhibited or TNFR1 signaling is otherwise impaired, caspase-8 becomes activated and causes cell death by apoptosis. Active caspase-8 can also cleave and thereby inhibit the receptor interacting serine-threonine protein kinase 1 and 3 (RIPK1 and RIPK3), thus blocking the necroptotic pathway. When caspase-8 is inhibited, for example by the viral FLIP-like proteins or by the synthetic caspase inhibitor QVD-OPH, TNFR1-induced apoptosis is inhibited, but the brake on the necroptotic pathway is also removed, allowing TNF to kill cells by necroptosis. Other proteins that influence the sensitivity of cells to necroptosis include cellular inhibitor of apoptosis proteins (cIAPs), which ubiquitylate and thereby inactivate RIP kinases, and deubiquitylating enzymes (DUBs), which deubiquitylate and thus activate RIP kinases (Vandenabeele et al., 2010). Experiments with gene-targeted mice have shown that the RIP kinases RIPK1 and RIPK3 are essential for TNF-induced necroptosis, and studies with RNAi-mediated knockdown or chemical inhibitors have also implicated the pseudokinase, mixed lineage kinase domain-like (MLKL), in this process (Sun et al., 2012; Wang et al., 2012; Zhao et al., 2012). However, the mechanism by which RIP kinases drive necroptosis, and the role of MLKL in this process, remain unclear.

MLKL is classified as a "pseudokinase" because its kinase-like domain lacks two of the three conserved catalytic residues considered crucial for phosphoryl transfer activity (Manning et al., 2002). Protein kinases rely on the Lys of the Val-Ala-Ile-Lys (VAIK) motif for interaction with the α and β phosphates of ATP to position ATP during phosphotransfer; on the Asp of the His-Arg-Asp (HRD) motif within the catalytic loop (subdomain VIb) to act as a catalytic residue; and on the Asp within the Asp-Phe-Gly (DFG) motif in the activation loop (subdomain VII)

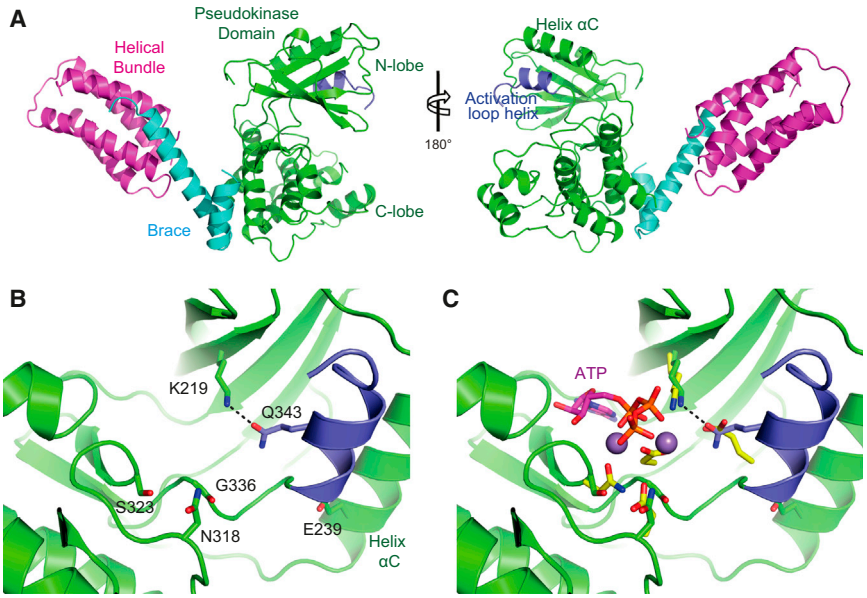

Figure 1. Structure of Mouse MLKL

(A) The structure of MLKL reveals an N-terminal helical bundle (magenta), a two-helix brace or linker (cyan), and a C-terminal pseudokinase domain (green). The activation loop helix, which forms part of the pseudokinase domain N-lobe, is colored in blue.

(B) Close-up of the pseudoactive site of MLKL reveals unusual coordination geometry for K219 in the VAIK motif. Instead of the classical kinase interaction with E239 of helix αC, it interacts with Q343 located on the atypical activation loop helix that occupies the canonical helix αC position. Other residues labeled correspond to deviations from residues typical for ATP binding and phospho-transfer in active protein kinases: G336 in MLKL replaces the Asp in the DFG motif responsible for Mg^{2+} coordination; N318 in MLKL replaces Asp of the HRD motif in the catalytic loop; and S323 that replaces the typical Asn located five residues C-terminal to the HRD motif usually involved in Mg^{2+} coordination.

(C) The pseudoactive site of MLKL overlaid with side chains of key residues within the active site of PKA (pdb 1ATP) (Zheng et al., 1993). Side chains for equivalent PKA residues to those described for MLKL are displayed in yellow, ATP is displayed in magenta, and Mn^{2+} (used in this structure as a surrogate for Mg^{2+}) displayed as spheres.

In all cases, oxygen atoms are displayed as red, nitrogen atoms as blue, and phosphorus atoms as orange. See also Figure S1 and Tables S1 and S2.

to bind Mg^{2+} to coordinate the β and γ phosphates of ATP (Hanks et al., 1988). In MLKL orthologs in chordate species, the VAIK motif is highly conserved but the HRD motif is absent and the DFG motif is degenerate and almost universally conserved as GFE. Pseudokinases comprise ~10% of mammalian kinomes and have emerged as regulators of cell signaling, acting predominantly as modulators of bona fide protein kinases (Boudeau et al., 2006; Saharinen and Silvennoinen, 2002; Zeqiraj and van Aalten, 2010). In some instances, pseudokinase domains, for example HER3 (Shi et al., 2010) and JAK2 (Ungureanu et al., 2011), have been observed to possess limited catalytic activity, although the generality of this phenomenon remains unclear (Eyers and Murphy, 2013).

We determined the crystal structure of full-length MLKL to 2.6 Å resolution revealing a four-helical bundle tethered to the pseudokinase domain. Generation of MLKL-deficient mice revealed that whereas under stress-free conditions, these animals are healthy, fertile, and ostensibly normal, cells derived from them were resistant to TNF-induced necroptotic cell death. We used MLKL-deficient cells reconstituted with inducible MLKL expression constructs to test the functional consequences of structure-guided mutations in MLKL. Mutations within the pseudoactive site of the pseudokinase induced constitutive necroptosis in the absence of TNF or other cytotoxic stimuli. These MLKL mutants were also constitutively active in *Ripk3*$^{-/-}$ fibroblasts. This illustrates that these mutants circumvent the requirement of RIPK3-mediated phosphorylation for activation and place RIPK3 upstream of MLKL in the necroptotic signaling pathway. Furthermore, the mitochondrial effector PGAM5 (Wang et al., 2012) did not appear to be necessary for necroptosis, suggesting that additional or alternative effectors must operate downstream of MLKL to induce necroptotic cell death.

RESULTS

MLKL Comprises an N-Terminal Four-Helix Bundle Tethered to the C-Terminal Pseudokinase Domain

The crystal structure of full-length murine MLKL was determined by X-ray diffraction at a resolution of 2.6 Å. The structure revealed that the N-terminal domain (amino acid residues 1 to 170) consists of a four-helix bundle followed by a two helix linker, or brace, connecting the bundle to the pseudokinase domain (residues 171 to 464, Figure 1A; crystallographic statistics in Table S1 available online). Additional studies with small-angle X-ray scattering confirmed that this unusual arrangement of domains is representative of MLKL in solution and not just within the crystal (Figures S1A–S1C; Table S2).

The C-terminal region of MLKL adopts a typical kinase-like fold, comprised of a smaller N-lobe made up of five antiparallel β strands and the helix αC and of the larger C-lobe composed principally of α helices. MLKL is classified as a pseudokinase based on the absence of Asp in the HRD motif of the catalytic loop and the absence of Asp in the DFG motif responsible for Mg^{2+} coordination (Figure S1D). Although the Lys within the ATP-binding VAIK sequence is conserved in MLKL, the structure reveals unusual coordination geometry for this residue (Figure 1B). Typically, in active protein kinases, this conserved Lys is positioned by a conserved Glu (E91 in cAMP-dependent protein kinase, PKA; E239 in MLKL) present on helix αC (Huse and Kuriyan, 2002; Taylor et al., 2012). However, in MLKL, the canonical helix αC position is occupied by an atypical α helix formed by the N-terminal segment of the MLKL activation loop (or "A-loop") comprising S340-I346 (colored blue in Figures 1A–1C). The activation loop of protein kinases is positioned in the cleft between the N- and C-lobes and begins after the canonical DFG motif in the N-lobe and extends into the C-lobe, providing a platform

for substrate binding (Huse and Kuriyan, 2002). The activation loops of protein kinases are typically very mobile, consistent with an absence of electron density for the residues K351-S358 in our MLKL structure. The MLKL activation loop helix occupies the position normally held by helix αC in conventional protein kinases and contributes Q343 to positioning the ATP binding lysine of the VAIK motif, in place of the helix αC glutamate typical of conventional kinases (Figure 1B). Despite this unusual arrangement, the ATP binding pocket is largely unaffected. A comparison between MLKL and PKA suggests that this pocket within MLKL should still be sufficiently large to accommodate ATP with minimal conformational rearrangements required (Figure 1C). Nevertheless, the absence of HRD and DFG motifs suggests that any such binding is unlikely to be catalytically productive; thus we refer to the cleft between the pseudokinase domain N- and C-lobes as the "pseudoactive" site in MLKL.

MLKL Binds ATP but Is a Catalytically Inactive Substrate of RIPK3

N-terminally His_6-tagged MLKL pseudokinase domain was expressed in insect cells and the recombinant protein purified by Ni^{2+}-affinity and size exclusion chromatography. Its ability to bind ATP, ADP, AMP, and the ATP analog AMPPNP in the presence or absence of Mg^{2+} or Mn^{2+} ions was tested in thermal stability shift assays. In these assays, ligand binding confers thermal stability to the protein, resulting in an increase in the melting temperature that can be measured by means of the dye Sypro Orange, which fluoresces upon binding to the hydrophobic surfaces exposed during protein denaturation (Lo et al., 2004; Lucet et al., 2013). Consistent with our prediction from the structure, we observed that wild-type MLKL bound ATP, ADP, and AMPPNP, but only in the absence of cations (Figures 2A and 2B). This binding was specific, because a mutant form of MLKL, in which the canonical ATP-binding lysine within the VTI$\underline{K}^{219}$ motif in the β3 strand was mutated to methionine (K219M), did not bind these ligands (Figures 2C and S2A). These data demonstrate that ATP binding occurs in the conventional ATP binding cleft between the MLKL pseudokinase N- and C-lobes. However, these data also suggest that MLKL is unlikely to function as a catalytically active protein kinase, because Mg^{2+} (or Mn^{2+}) is known to play an essential role in the phosphoryl transfer mechanism of protein kinases.

The active sites of conventional, catalytically active protein kinases utilize an ion pair between the lysine of the VAIK motif and a glutamate in the helix αC to position the lysine for interaction with the α- and β-phosphates of ATP during catalysis. In contrast, in MLKL, K219 of the VTI$\underline{K}$ motif forms a hydrogen bond with Q343, a residue within the unusual activation loop helix, rather than ion pairing with the canonical helix αC glutamate, E239. Both the Q343A and E239A mutant forms of MLKL retained ATP binding capacity (Figures 2D and S2B–S2D). This indicates that ATP binding does not result from a conformational change that repositions E239 of helix αC to interact with K219 and that Q343 plays an auxiliary, rather than an obligate, role in positioning K219 for ATP binding.

We further explored the relationship between MLKL and RIP kinases in necroptosis by using biochemical techniques. Although we did not detect an interaction between MLKL immunoprecipitated from mouse dermal fibroblasts (MDFs) and endogenous RIPK1 or RIPK3 (Figure S2E) or between recombinant MLKL and RIPK3 in isothermal titration calorimetry experiments (not shown), recombinant RIPK3 kinase domain robustly phosphorylated the MLKL pseudokinase domain within 5 min of initiating an in vitro γ-[^{32}P]ATP kinase assay (Figure 2E). The MLKL pseudokinase domain did not autophosphorylate (lanes 2 and 7, autoradiograph Figure 2E), consistent with its predicted lack of catalytic activity. In control experiments with recombinant RIPK3 harboring the kinase-inactivating mutation, D143N, expressed and purified in the same manner as wild-type RIPK3, we observed no MLKL phosphorylation (Figure S2F), demonstrating that RIPK3 rather than a trace contaminant mediates MLKL phosphorylation. By using mass spectrometry, we identified S345, S347, and T349 within the MLKL activation loop as the sites of RIPK3 phosphorylation (Figures 2F and S2G–S2I). These data imply a transient substrate:kinase interaction between MLKL and RIPK3.

MLKL Is Required for Necroptosis

To explore the physiological functions of MLKL, we generated *Mlkl*-deficient mice. A targeting vector was constructed for generation of a modified *Mlkl* allele via homologous recombination in C57BL/6 embryonic stem cells (ESCs) (Figure 3A), allowing Cre-dependent deletion of exon 3. Chimeric mice were generated from an ESC clone bearing the targeted locus and heterozygous offspring were bred to *deleter* cre-expressing mice (Schwenk et al., 1995). Intercrosses of mice heterozygous for the cre-deleted *Mlkl* allele ($Mlkl^{-}$) yielded mice of each of the three expected genotypes in Mendelian ratios (21% $Mlkl^{+/+}$, 50% $Mlkl^{+/-}$, 29% $Mlkl^{-/-}$, n = 24). Immunoblots of protein extracts from a range of organs demonstrated that MLKL was readily detectable in all organs, except the brain, in wild-type mice, with particularly high levels evident in the bone marrow. MLKL protein was absent in all tissues of homozygous mutant mice, verifying functional deletion of the *Mlkl* gene (Figure 3B).

$Mlkl^{-/-}$ mice appeared outwardly indistinguishable from their heterozygous and wild-type littermates and histological examination of their major organs revealed no abnormalities. Peripheral blood cell numbers in $Mlkl^{-/-}$ mice were within normal ranges and enumeration of myeloid progenitor cells by colony formation in semisolid medium revealed no numerical or morphological anomalies in colonies grown from either the bone marrow or spleen (Table S3). The number of cells in the lineage^{-}Sca-1^{+}c-Kit^{+} (LSK) fraction of the bone marrow, which contains the hematopoietic stem cells, was also normal in $Mlkl^{-/-}$ mice (Figure S3A). In competitive transplantation assays, $Mlkl^{-/-}$ stem cells were able to compete as effectively as their wild-type counterparts for long-term reconstitution of the hematopoietic system of myeloablated transplant recipients (Figure S3B).

In siRNA experiments, MLKL has recently been implicated in TNF-induced necroptosis (Sun et al., 2012; Zhao et al., 2012). Consistent with this observation, we found that $Mlkl^{-/-}$ mouse dermal fibroblasts (MDFs), mouse embryonic fibroblasts (MEFs), and bone-marrow-derived macrophages (BMDMs) were resistant to necroptosis induced by the combination of TNF (T), Smac-mimetic (S), and the caspase-inhibitor QVD-OPH (Q), in clear contrast to their wild-type counterparts (TSQ

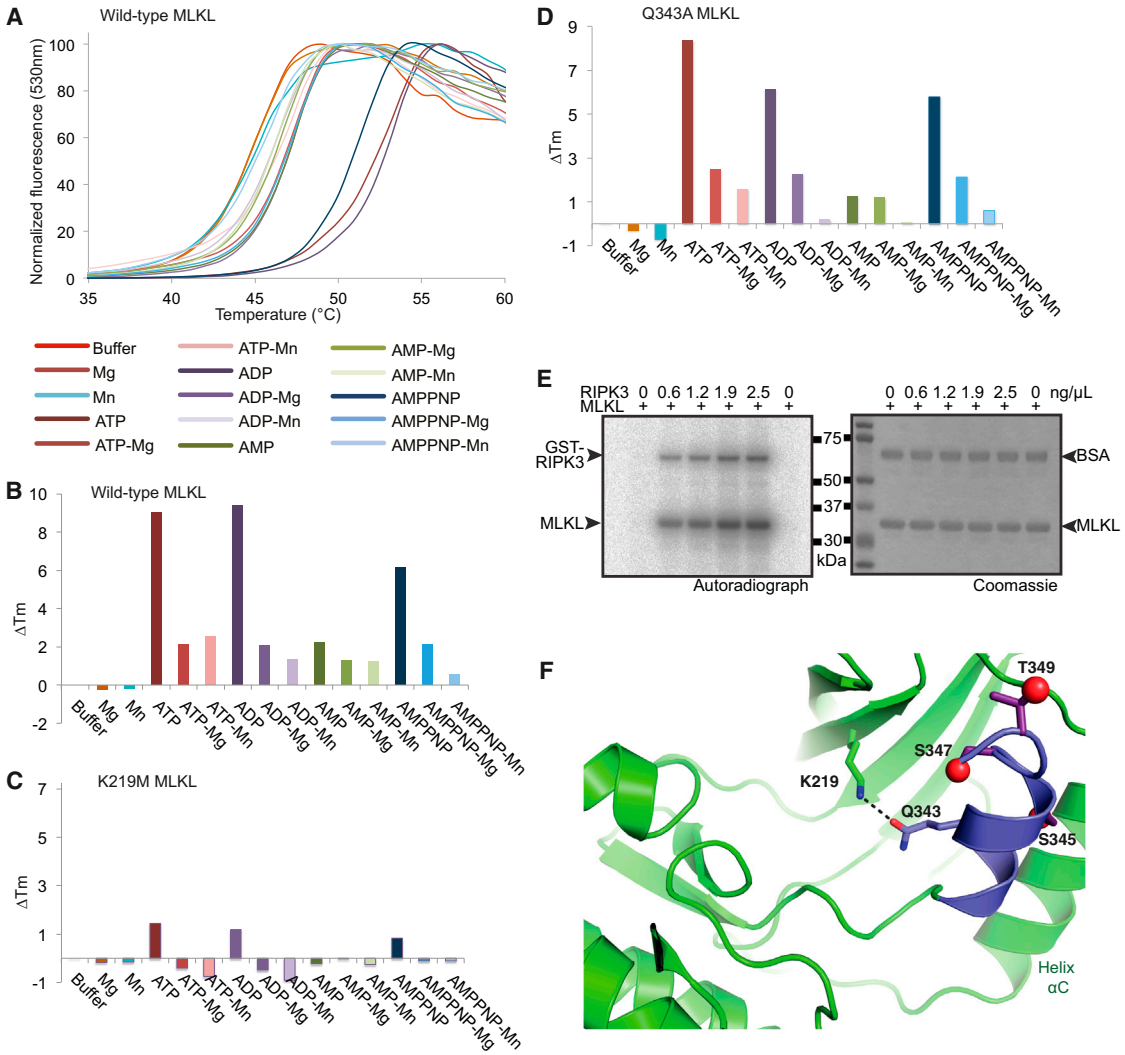

Figure 2. Recombinant MLKL Binds ATP In Vitro and Is a Catalytically Inactive Substrate of RIPK3

(A) Nucleotide binding by His_6-tagged wild-type MLKL pseudokinase domain in the presence or absence of Mn^{2+} or Mg^{2+} was determined with a thermal stability shift assay. The plot is representative of three independent experiments.

(B) A bar graph analysis of the data presented in (A) (as described in Experimental Procedures).

(C and D) Thermal stability shifts measured for K219M (C) and Q343A (D) mutant forms of the MLKL pseudokinase domain in the presence or absence of nucleotides and cations. Each plot is representative of at least two independent experiments. Corresponding thermal stability curves are shown in Figure S2.

(E) Recombinant MLKL pseudokinase domain (125 ng/μl) was subjected to γ-[^{32}P]ATP kinase assays in the presence or absence of increasing concentrations of recombinant GST-RIPK3 kinase domain. Control experiments performed with recombinant RIPK3 harboring the inactivating mutation D143N are shown in Figure S2F. Data shown are representative of three independent experiments. BSA was added as a carrier protein (100 ng/μl).

(F) S345, S347, and T349 in the MLKL activation loop were phosphorylated by RIPK3 in in vitro kinase assays. Cartoon of MLKL pseudoactive site (drawn in the same orientation as in Figures 1B and 1C); red spheres represent oxygen atoms that are phosphorylated. See Figures S2G–S2I.

treatment, Figures 4A–4C and S4). Importantly, reconstitution of full-length MLKL via an inducible lentiviral expression vector restored the sensitivity of *Mlkl*$^{-/-}$ MDFs to TNF-induced necroptosis (Figures 4D–4F).

MLKL Pseudoactive Site Mutants Induce Necroptosis in the Absence of Exogenous Stimuli and Independently of RIPK3 Activity

The crystal structure of MLKL revealed an unusual organization of residues in the pseudoactive site. In particular, the atypical activation loop helix residue Q343 coordinates the conventional ATP binding residue K219 (Figure 1B). We therefore sought to establish the role of Q343 and its interactor, the key ATP-binding lysine K219, in vivo.

Induced expression of K219M MLKL restored normal sensitivity to TSQ-induced necroptosis in *Mlkl*$^{-/-}$ MDFs (Figure 5A). Because the K219M mutant was unable to bind ATP (Figures 2C and S2A), this result demonstrates that ATP binding is dispensable for MLKL-dependent necroptosis. Interestingly, there was also an indication of increased cell death in the *Mlkl*$^{-/-}$ MDFs when expression of the K219M mutant was induced in the absence of other stimuli, and this was even more striking in

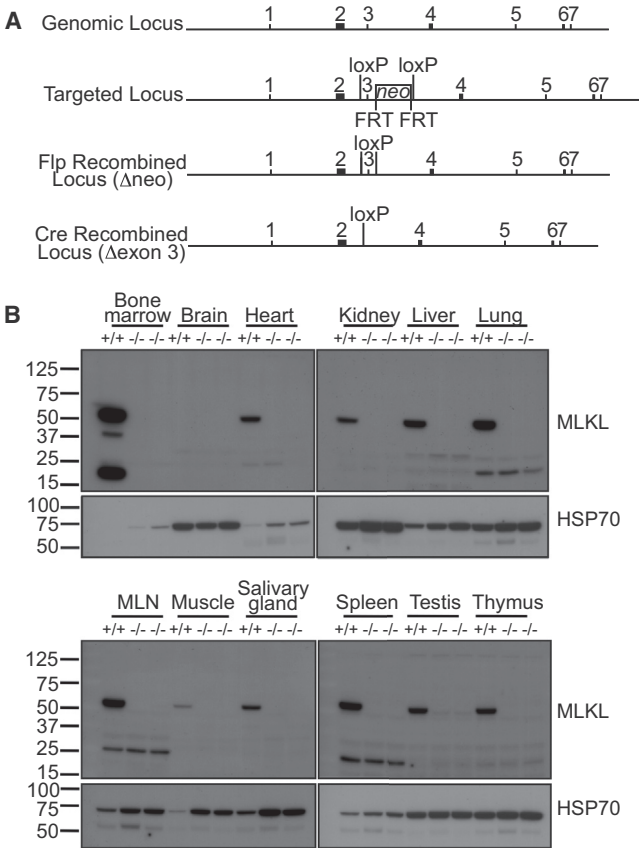

Figure 3. Functional Deletion of the *Mlkl* Gene in Mice

(A) Gene targeting strategy for the generation of MLKL-deficient mice. The location of exons is indicated by raised, numbered boxes. A targeting vector, in which an *frt*-flanked neomycin resistance cassette was inserted in intron 3 of the *Mlkl* genomic locus along with *loxP* sites upstream of exon 3 and immediately downstream of the resistance cassette, was used to generate the targeted locus in ESCs via homologous recombination. Mice bearing the targeted locus were bred with *deleter* cre-expressing mice (Schwenk et al., 1995) to generate mice heterozygous for the recombined Δ-exon 3 locus ($Mlkl^{+/-}$ mice). These heterozygous $Mlkl^{+/-}$ mice were intercrossed to produce homozygous $Mlkl^{-/-}$ mice. See also Figure S3 and Table S3.

(B) Immunoblot for MLKL protein on extracts of tissues from two $Mlkl^{-/-}$ (−/−) mice and one wild-type (+/+) mouse. Wild-type (+/+) immunoblots are representative of three independent experiments. After probing for MLKL, blots were stripped and reprobed with antibodies to HSP70 (loading control, bottom). Molecular weight markers (kDa) are indicated at the left.

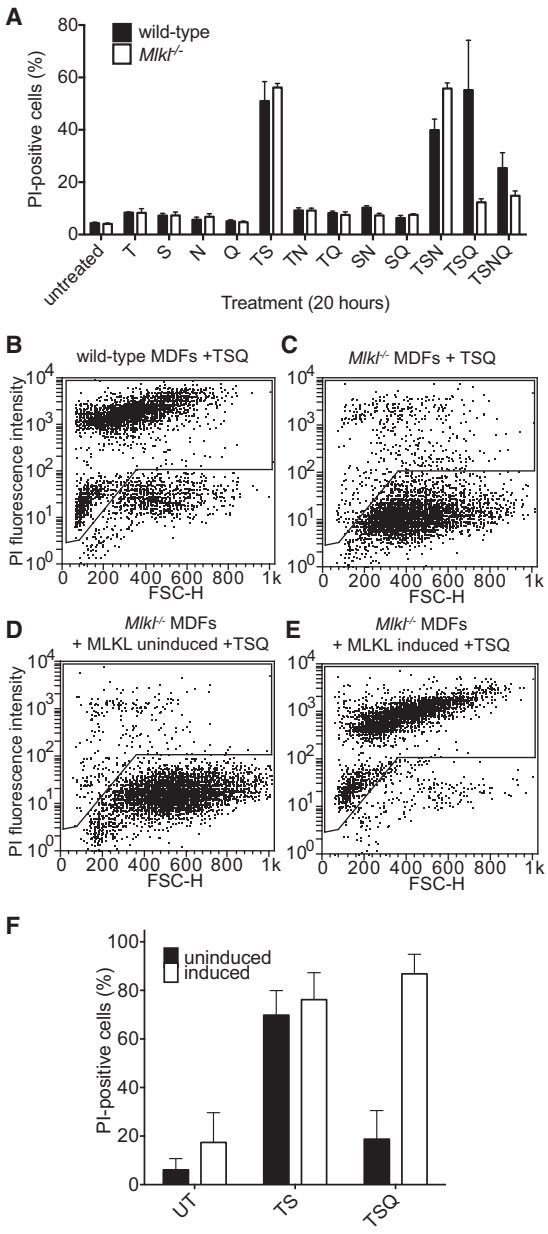

Figure 4. Sensitivity of $Mlkl^{-/-}$ MDFs to Necroptotic Stimuli

(A) MDF cell lines derived from wild-type or $Mlkl^{-/-}$ mice were treated with necroptosis-inducing stimuli as indicated for 20 hr. Abbreviations are as follows: T, TNF; S, Smac-mimetic; N, Necrostatin-1; Q, QVD-OPH. Cell death was measured by enumerating PI permeable cells with flow cytometry.

(B–E) Representative flow cytometry plots of wild-type MDFs (B), $Mlkl^{-/-}$ MDFs (C), and $Mlkl^{-/-}$ MDFs reconstituted with inducible wild-type MLKL off (D) or on (E) stimulated by TSQ treatment and stained with PI. Data are representative of at least three biological replicates.

(F) TSQ-treated $Mlkl^{-/-}$ MDFs inducibly expressing (white bars) or not expressing (black bars) MLKL. UT, untreated.

Data are plotted as the mean ± SD of at least three biological replicates. See also Figure S4.

wild-type MDFs induced to express K219M MLKL (Figure 5B). We obtained similar, but more pronounced, results with a Q343A mutant MLKL, which cannot hydrogen bond with K219, because inducible expression of this mutant caused significant cell death in both $Mlkl^{-/-}$ (Figure 5C) and wild-type (Figure 5D) MDFs. Immunoblot analysis confirmed that expression of the K219M and Q343A MLKL mutants was comparable to that of inducibly expressed wild-type MLKL (Figure S5D), which did not induce TSQ-independent cell death. This demonstrates that perturbations to the pseudoactive site, rather than disparate expression levels, underlie the constitutive necroptosis-inducing activity of these mutants. Enforced overexpression of certain proteins can cause apoptosis. It was therefore possible that the death induced by enforced expression of the MLKL mutants might be different from necroptotic death induced by stimulation with TSQ. The broad-spectrum caspase inhibitor QVD-OPH had

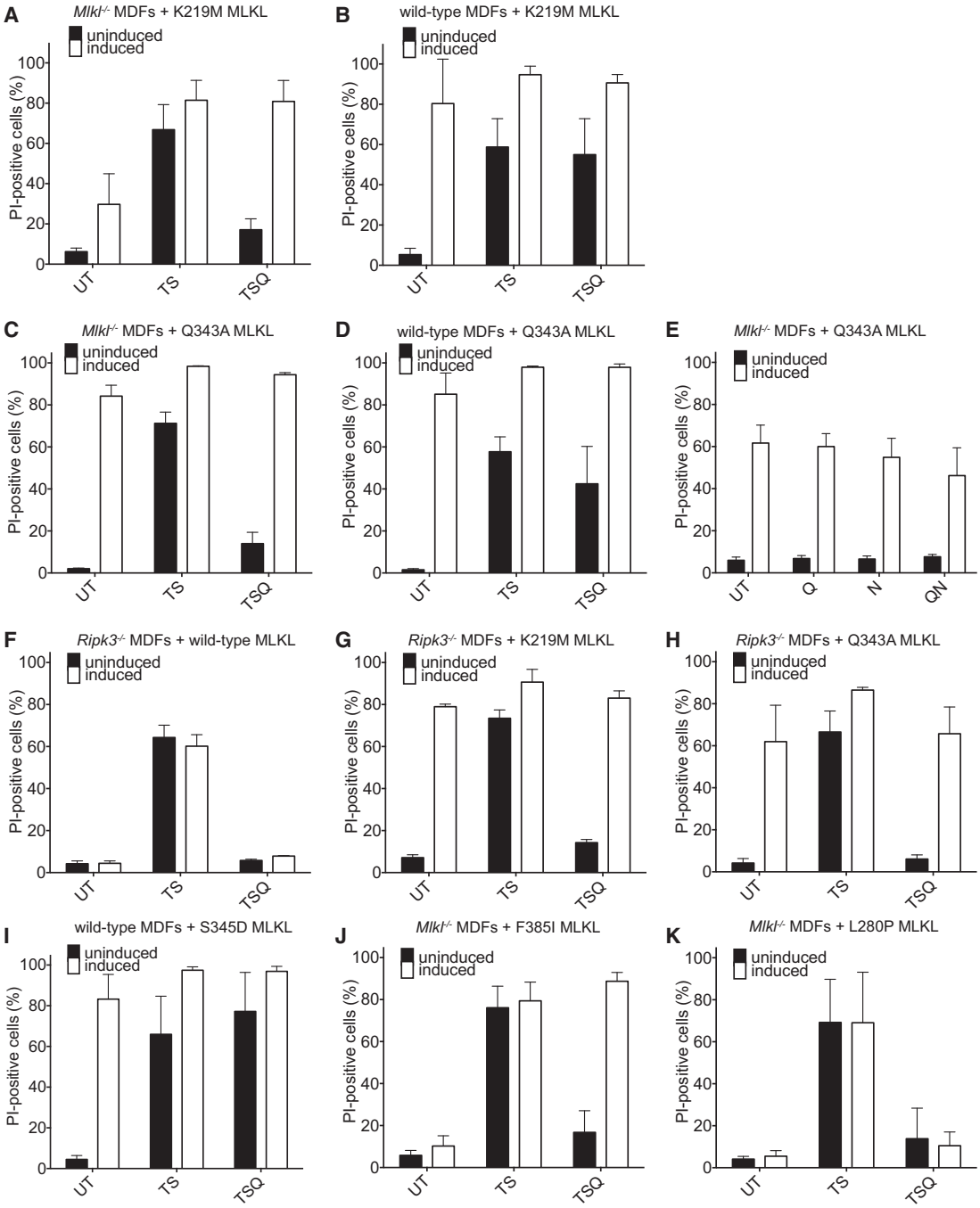

Figure 5. Cell Death of *Mlkl*$^{-/-}$, Wild-Type, and *Ripk3*$^{-/-}$ MDFs Inducibly Expressing Pseudoactive Site Mutants of MLKL

(A and B) A K219M mutant MLKL was inducibly expressed in *Mlkl*$^{-/-}$ MDFs (A) or wild-type MDFs (B) ± TS (apoptotic stimulus) or TSQ (necroptotic stimulus) and cell death quantitated by PI staining and flow cytometry. Abbreviations are as follows: UT, untreated; T, TNF; S, Smac-mimetic; Q, QVD-OPH.

(C and D) A Q343A mutant MLKL was inducibly expressed in *Mlkl*$^{-/-}$ (C) or wild-type MDFs (D) and treated and assayed as in (A).

(E) A Q343A mutant MLKL was inducibly expressed in *Mlkl*$^{-/-}$ MDFs ± QVD-OPH (Q), Nec-1 (N), or QVD-OPH plus Nec-1 (QN).

(F–H) *Ripk3*$^{-/-}$ MDFs with inducible wild-type (F), K219M (G), or Q343A (H) MLKL ± TS or TSQ were stained with PI staining and cell death quantitated by flow cytometry.

(I) The phosphomimetic S345D mutant MLKL was inducibly expressed in wild-type MDFs and death in the presence or absence of apoptotic or necroptotic stimuli quantitated by PI staining and flow cytometry.

(J and K) The mouse counterparts of MLKL mutations identified in human stomach cancer, F385I (J) and L280P MLKL (K), were inducibly expressed in *Mlkl*$^{-/-}$ MDFs and their sensitivity to apoptotic and necroptotic stimuli examined. Positions of these mutations within the MLKL structure are shown in Figure S1E.

In all panels, cell lines were treated as indicated and 24 hr later PI-positive cells were quantitated via flow cytometry. The results represent the mean ± SD from three independently derived MDF cell lines, each tested one to three times. See also Figure S5.

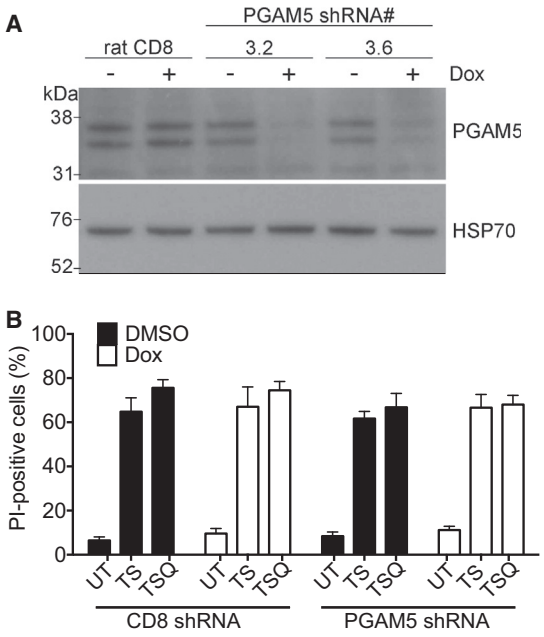

Figure 6. Sensitivity of Wild-Type MEFs to Necroptotic Stimuli after shRNA Knockdown of PGAM5

(A) Wild-type MEFs stably transfected with doxycycline-inducible shRNAs targeting PGAM5 were treated with doxycycline and after 72 hr immunoblot was used to measure knockdown efficiency compared to a rat CD8 shRNA control. Two independent clones were used in these studies. HSP70 was used as a loading control.

(B) Wild-type MEFs stably expressing shRNAs against PGAM5 were treated with 100 ng/ml TNF (T), 500 nM Smac mimetic (S), and 25 μM QVD (Q) or left untreated (UT), as indicated. Cell viability was determined after 24 hr of treatment by PI staining and flow cytometry. Data are represented as the mean ± SEM of at least three independent experiments.

Parallel experiments with L929 cells are shown in Figure S6.

no effect on Q343A mutant MLKL-induced cell death, demonstrating that overexpression of this mutant does not cause apoptosis (Figure 5E). RIPK1 would be expected to act upstream of MLKL in necroptosis signaling and, accordingly, the RIPK1 inhibitor Nec-1 had no effect on Q343A mutant MLKL-induced cell killing either alone or in the presence of the caspase inhibitor QVD-OPH (Figure 5E), although these inhibitors were functional in blocking TSQ-induced necroptosis and TS-induced apoptosis in these cells (Figure S5A). The small amount of cell death caused by induced expression of wild-type MLKL in *Mlkl*$^{-/-}$ MDFs was likewise unaffected by QVD-OPH or Nec-1 (Figure S5B), despite the fact that these inhibitors blocked TSQ-induced necroptosis and TNF/cycloheximide-induced apoptosis in these same cells (Figure S5C).

During TSQ-induced necroptosis, MLKL is thought to act downstream of RIPK3 (Sun et al., 2012; Zhao et al., 2012). As previously described for RIPK3-deficient cells (He et al., 2009), our *Ripk3*$^{-/-}$ MDFs were insensitive to TSQ-induced necroptosis (Figure 5F). Consistent with the notion that RIPK3 acts upstream of MLKL, inducible overexpression of wild-type MLKL was unable to restore sensitivity of these *Ripk3*$^{-/-}$ fibroblasts to necroptotic stimuli (Figure 5F). In contrast, but consistent with the notion that MLKL acts downstream of RIPK3, expression of the K219M or Q343A mutant forms of MLKL caused substantial necroptosis in RIPK3-deficient cells in the absence of any additional stimulus (Figures 5G and 5H). We then examined whether substitution of the MLKL activation loop residue S345 with Asp, to mimic phosphorylation by RIPK3 conferred a similar phenotype on MDFs as the pseudoactive site mutants. Indeed, S345D mutant MLKL expression in wild-type (Figure 5I) and *Mlkl*$^{-/-}$ (not shown) MDFs led to cell death in the absence of necroptotic stimuli. These data suggest that the K219M and Q343A pseudoactive site mutations cause a conformational change within MLKL that mimics RIPK3-mediated activation of MLKL to induce spontaneous, RIPK3-independent necroptosis.

Two mutations in highly conserved residues located within the C-lobe of the MLKL pseudokinase domain, F398I and L291P (F385 and L280 in mouse MLKL) (Figures S1D and S1E), have been identified in human stomach adenocarcinoma samples (Forbes et al., 2008). Although the F385I MLKL mutant showed wild-type activity when inducibly expressed in *Mlkl*$^{-/-}$ cells treated with TSQ (Figure 5J), the L280P MLKL mutant failed to restore sensitivity to this necroptotic stimulus (Figure 5K), despite being expressed at comparable levels to endogenous MLKL (Figure S5D). This suggests that, owing to a likely structural perturbation within the C-lobe of the MLKL pseudokinase domain (Figure S1E), L280P represents a loss-of-function mutation of MLKL.

The Mitochondrial Protein PGAM5 Is Dispensable for RIPK3-MLKL-Mediated Necroptosis

The mitochondrial phosphatase PGAM5 was reported to be a critical downstream effector both of necroptosis induced by TNFR1 > RIPK1 > RIPK3 > MLKL signaling and of necroptosis induced by cytotoxic stimuli that are independent of these signal transducers, such as H_2O_2 or ionomycin (Wang et al., 2012). We sought to further define the role of PGAM5 in the RIPK3 > MLKL necroptosis signaling pathway by knocking down expression of PGAM5 by using shRNA in wild-type MEFs and L929 fibroblastoid cells (Figures 6A, S6A, and S6B). Intriguingly, cells in which a PGAM5 shRNA or a nonsilencing control shRNA were expressed were equally susceptible to TSQ-induced necroptosis (Figures 6B and S6C). This suggests that additional or alternative pathways must operate in RIPK3 > MLKL-mediated necroptosis.

DISCUSSION

Necroptosis is a form of programmed cell death that occurs when apoptosis and caspase activity are inhibited. Because this constitutes a mechanism that may allow elimination of pathogens that are able to subvert classical apoptotic cell death or as a failsafe in other situations where the preferred apoptosis pathway fails, there has been considerable interest in defining the molecular regulators of necroptosis and their mechanisms of action. Recent evidence suggests that necroptosis is dependent on the RIP kinases RIPK1 and RIPK3 (Cho et al., 2009; Degterev et al., 2005; Duprez et al., 2011; He et al., 2009); the MLKL pseudokinase has also been implicated as a key mediator downstream of RIPK3 (Sun et al., 2012; Zhao et al., 2012). To define the function of MLKL in a physiological context, we generated mice lacking a functional *Mlkl* gene. Although devoid of

detectable MLKL protein in all tissues examined, in the absence of stress *Mlkl*$^{-/-}$ mice were healthy and fertile, with no apparent pathological abnormalities or hematological disturbance. Cells derived from *Mlkl*$^{-/-}$ mice were, however, completely resistant to TSQ-induced necroptosis, and normal sensitivity could be restored upon reconstitution of MLKL expression. This demonstrates an essential role for MLKL in necroptosis. This contrasted with the absence of any effect on the sensitivity of cells to necroptosis upon shRNA-mediated reduction in the expression of the phosphatase PGAM5. This suggests that pathways acting in a manner redundant with, or instead of, PGAM5 are critical for necroptosis, at least within the cells studied here.

The lack of an overt phenotype in unstressed *Mlkl*$^{-/-}$ mice in our study is consistent with a recent report describing *Mlkl*-deficient mice generated by the TALEN approach (Wu et al., 2013) and is similar to observations made with mice lacking RIPK3 (Newton et al., 2004), a critical regulator of TNF-induced necroptosis thought to act upstream of MLKL. RIPK3-deficient mice were, however, reported to show abnormal inflammatory responses during vaccinia virus infection (Cho et al., 2009), cerulein-induced acute pancreatitis (He et al., 2009), and TNF administration (Duprez et al., 2011). Together, these data show that RIPK3 is required for induction of necroptosis and suggest that RIPK3-MLKL-driven cell death is more important in response to the challenges of infection or pathological inflammation than in steady-state homeostasis. Although our data clearly implicate MLKL as a crucial effector of TNF-induced necroptotic signaling, a recent study showed that MLKL contributes to inflammasome activation (Kang et al., 2013), raising the exciting possibility that MLKL, like RIPK3, may serve important functions in other signaling pathways. A potential role for MLKL in neoplastic disease was raised by the identification of mutations in highly conserved residues within the MLKL pseudokinase domain in human stomach adenocarcinoma (Forbes et al., 2008). Our observation that one of these mutations, MLKL L280P, lacks activity in MLKL-induced necroptosis assays strengthens this notion and implies that further investigation of MLKL as a potential tumor suppressor in some cancer contexts is warranted.

To better define the molecular mechanism by which MLKL acts, we solved the crystal structure of full-length mouse MLKL to 2.6 Å resolution. This structure revealed MLKL to be composed of an N-terminal four-helix bundle braced to the C-terminal pseudokinase domain via a two helix linker. Of particular interest, the pseudokinase domain contained an atypical helix in the activation loop that packed against the N-lobe αC helix. This prevents the formation of the canonical ionic bond between the lysine of the VAIK motif (K219) and the helix αC glutamate (E239), an interaction that is synonymous with an active protein kinase conformation. In place of the helix αC glutamate, the residue Q343 that is within the unusual activation loop helix hydrogen bonds K219. An examination of MLKL amino acid sequences among orthologs revealed that K219 is almost universally conserved and that Q343 is present as Gln or Glu (Figure S1D). The one exception to the conservation of K219 was in *O. garnettii* MLKL where a charge reversal was present: the K219 position was substituted with Glu and the Q343 position with Lys. Collectively, these data suggest that orthologs of K219 and Q343 serve important functions in MLKL.

As predicted from the crystal structure, the MLKL pseudokinase domain was capable of nucleotide binding, though only in the absence of Mg^{2+} and Mn^{2+}. As anticipated, nucleotide binding was lost upon mutation of the canonical ATP-binding residue K219. Although the VAIK motif Lys is typically thought of as a catalytic, rather than ATP-binding, residue in active protein kinases (Carrera et al., 1993), recent studies suggest that pseudokinase domains have evolved mechanisms of ATP binding divergent from bona fide protein kinases. For example, mutation of the VAIK motif in the pseudokinase domain of HSER/GC-C has previously been shown to abrogate ATP binding (Jaleel et al., 2006). Consistent with the notion that pseudokinase domains have evolved unconventional ATP binding modes, we observed that Mg^{2+} and Mn^{2+} thwarted ATP binding by MLKL. Because divalent cations play an essential role in catalyzing the kinase reaction, it is therefore unlikely that MLKL will function as a catalytically active protein kinase. Indeed, MLKL at very high concentrations (125 ng/μl) exhibited no autophosphorylation in in vitro kinase assays, an observation consistent with a previous report (Sun et al., 2012), but was a substrate of recombinant RIPK3 in the same in vitro kinase assays. Coimmunoprecipitation and isothermal titration calorimetry studies failed to detect a stable complex containing RIPK3 and MLKL, suggesting that their interaction was transient and typical of an enzyme:substrate complex. Thus, we propose that MLKL, activated by RIPK3-mediated phosphorylation, is likely to serve as a substrate of the necrosome rather than as a catalytically active kinase. Indeed, the K219M mutant form of MLKL that cannot bind ATP restored normal sensitivity to necroptotic stimuli (TSQ) in *Mlkl*$^{-/-}$ MDFs. Although one report has suggested that MLKL can function as a kinase (Zhao et al., 2012), these studies used MLKL immunoprecipitated from 293T cells, making it possible that the weak activity they observed was from a kinase that had coprecipitated with MLKL. Our data support the idea that pseudokinases play important, nonenzymatic roles in cellular signaling and demonstrate that neither ATP binding nor kinase activity is crucial for MLKL function in necroptosis.

Inducible expression of the K219M MLKL mutant triggered necroptosis in MDFs in the absence of TSQ treatment. This constitutive necroptosis-inducing activity was recapitulated by a mutation perturbing Q343, the binding partner of K219 in the MLKL pseudoactive site. The absence of definitive markers makes it difficult to conclude that the death induced by Q343A or K219M mutant forms of MLKL is definitively necroptotic, but this death could not be blocked by inhibition of caspases or RIPK1. Moreover, although inducible expression of wild-type MLKL did not restore sensitivity to necroptotic stimuli in *Ripk3*$^{-/-}$ MDFs, expression of comparable levels of K219M or Q343A mutant forms of MLKL killed these *Ripk3*$^{-/-}$ MDFs in the absence of any stimuli. These data are consistent with the notion that the K219M and Q343A mutations subvert the need for RIPK3 phosphorylation to activate the necroptotic activity of MLKL. Based on these observations, we propose that structural changes in the MLKL activation loop are normally induced by RIPK3-mediated phosphorylation, which in turn alter the conformation of the MLKL pseudoactive site to cause necroptosis. This is further supported by the proximity of Q343 to the MLKL activation loop residues that we identified as substrates of RIPK3 phosphorylation (S345, S347, and T349) and the

observation that the phosphomimetic mutant S345D could induce necroptosis signaling in the absence of stimuli. These data support a model in which the MLKL mutants K219M and Q343A emulate the activation loop perturbations usually induced by RIPK3-mediated phosphorylation, circumventing the requirement for RIPK3 phosphorylation and allowing spontaneous necroptosis. Thus, MLKL phosphorylation by RIPK3 constitutes a critical checkpoint in necroptosis signaling.

EXPERIMENTAL PROCEDURES

Expression Constructs

The mouse MLKL cDNA encoding residues 1–464 was PCR amplified from a reverse-transcribed cDNA library derived from G1ME cells (Stachura et al., 2006) and ligated into pBlueScript SK or obtained as a synthetic DNA in which several restriction sites were eliminated by silent substitutions (DNA2.0). Mutations were introduced into the MLKL cDNA by oligonucleotide-directed PCR mutagenesis. DNA oligonucleotides encoding shRNA sequences targeting PGAM5 were designed and cloned into the dox-inducible lentiviral expression vector FH1tUTG. Details can be found in the Supplemental Experimental Procedures.

Recombinant Protein Expression and Purification

cDNAs encoding *Mus musculus* MLKL 1–464 or 179–464 with and without mutations were cloned into the pFastBac HTb vector (Life Technologies). A cDNA encoding mouse RIPK3 kinase domain was cloned into either pFastBac HTb or a derivative of pFastBac1 incorporating an N-terminal GST tag. For details of expression and purification methods, see Supplemental Experimental Procedures. Selenomethionine incorporation into MLKL 1–464 for crystallographic phasing was based on a published method (Cronin et al., 2007), with further details in Supplemental Experimental Procedures.

Crystallization and Structure Determination

Full-length MLKL was concentrated to 5 mg/ml and subjected to robotic crystal trials (C3 Facility, CSIRO). Initial screens yielded small needles that were optimized to produce larger needles as outlined in Supplemental Experimental Procedures. X-ray diffraction data were collected at the Australian Synchrotron beamline MX2 at 100K. Data were processed with HKL2000 (Otwinowski and Minor, 1997) and the structure solved by SAD with autoSHARP (Vonrhein et al., 2007) with data collected from crystals soaked in 2 mM $UO_2(NO_3)_2$ before freezing. Initial building with Arp/Warp (Langer et al., 2008) and refinement with REFMAC5 (Murshudov et al., 2011) provided regions of model and maps sufficient in detail to identify the pseudokinase region. Subsequent rounds of building with COOT (Emsley et al., 2010) and refinement with Phenix (Adams et al., 2010), guided in part by comparison to published kinase structures, provided an early model that was subsequently refined against higher-resolution native data. Building of the novel N-terminal domain was further assisted by the identification of methionine residues in anomalous difference maps produced in Phenix (Adams et al., 2010) with data from selenomethionine-incorporated crystals. Small-angle X-ray scattering data were collected as described in the Supplemental Experimental Procedures with parameters shown in Table S2. All structure cartoons were drawn with Pymol.

Thermal Shift Assay for Nucleotide Binding

The thermal stability shift assay was conducted with a Corbett Real Time PCR machine as detailed in the Supplemental Experimental Procedures.

Generation of MLKL-Deficient Mice

Homologous recombination in ESCs was used to generate a conditionally targeted *Mlkl* locus with exon 3 flanked by loxP sites. Additional details and the methods used to generate homozygous Δ-exon 3 *Mlkl*$^{-/-}$ mice on an inbred C57BL/6 background, as well as PCR-based genotyping, can be found in the Supplemental Experimental Procedures. Animal experiments were performed according to protocols approved by the Walter and Eliza Hall Institute of Medical Research Animal Ethics Committee.

Histological and Hematological Analysis

Histological and hematological analyses of *Mlkl*$^{-/-}$ mice were performed according to published methods (Alexander et al., 1996), with additional details provided in Supplemental Experimental Procedures.

Reagents and Antibodies

Recombinant hTNF-Fc was produced in-house as described (Bossen et al., 2006). Puromycin, doxycycline, necrostatin-1, and cycloheximide were purchased from Sigma-Aldrich. The Smac mimetic Compound A has been described previously (Vince et al., 2007). QVD-OPH was purchased from R&D Systems. A monoclonal rat anti-mouse MLKL antibody (clone 3H1) was raised in-house by the Walter and Eliza Hall Institute Monoclonal Facility by immunizing Wistar rats with the peptide CQPASWQQEDRQDAEED, conjugated to keyhole limpet hemocyanin. Anti-β-actin antibody was purchased from Sigma Aldrich; anti-HSP70 antibody was purchased from Santa Cruz or kindly provided by R. Anderson, Peter MacCallum Cancer Research Centre; rabbit polyclonal anti-PGAM5 antibody was kindly provided by Z. Wang, UT Southwestern Medical Center at Dallas (Wang et al., 2012); rabbit anti-RIPK3 antibody was purchased from ProSci; and mouse anti-RIPK1 antibody was purchased from BD Biosciences. HRP-conjugated secondary antibodies were purchased from GE Healthcare and Jackson Immunoresearch. Immunoprecipitations and immunoblot analysis were performed as described in the Supplemental Experimental Procedures.

Cell Lines and Cell Death Assays

Mouse embryonic fibroblasts (MEFs) derived from *Mlkl*$^{-/-}$ or wild-type mice were generated from E14.5 embryos and immortalized with SV40 large T antigen. MEFs, HEK293T, and L929 cells were maintained in Dulbecco's modified Eagle's medium (DMEM) supplemented with 8%–10% fetal calf serum (FCS) and 5 μg/ml puromycin for lines stably transduced with inducible expression constructs for MLKL. Mouse dermal fibroblasts and mouse embryonic fibroblasts were isolated from three *Mlkl*$^{-/-}$ mice and three congenic wild-type mice and then immortalized by SV40 large T antigen to generate three biologically independent cell lines. Immortalized MDFs were similarly prepared from three *Ripk3*$^{-/-}$ mice and congenic wild-type mice. Cell death assays were carried out in 24-well plates, seeding 1 × 10^5 cells per well. Cells attached over 4 hr in the presence of 10 ng/ml doxycycline were then treated with assorted combinations of cycloheximide (250 ng/ml), necrostatin (50 μM), and QVD-OPH (5 μM) 30 min prior to addition of TNF (100 ng/ml) and Smac mimetic (500 nM). After 24 hr, cells were harvested and PI-positive cells (100 ng/ml) were quantified with a BD FACSCalibur flow cytometer. For assessment of the effects of PGAM5 knockdown, MEFs or L929 cells were treated with doxycycline to induce the expression of the short hairpins. After 48 hr, cells were seeded into 24-well plates at 5 × 10^4 cells per well and the following day were treated with TNF, Smac mimetic, and QVD-OPH. After 24 hr, adherent cells were stained with PI and assessed by flow cytometry. BMDM cell suspensions from bone marrow were cultured for 6 days in DME supplemented with 10% FCS and 20% L929 conditioned medium. At day 6 the resulting BMDMs were plated at 5 × 10^5 cells per well in a 24-well plate and the following day were treated with TNF, Smac mimetic, and QVD-OPH. After 24 hr, adherent cells were stained with PI and assessed by flow cytometry.

Statistical Analyses

Error bars represent mean ± SD (Figures 4 and 5) or mean ± SEM (Figure 6).

ACCESSION NUMBERS

The atomic coordinates and structure factors for MLKL (PDB ID code 4BTF) have been deposited in the Protein Data Bank, Research Collaboratory for Structural Bioinformatics, Rutgers University (http://www.rcsb.org).

SUPPLEMENTAL INFORMATION

Supplemental Information includes Supplemental Experimental Procedures, six figures, and three tables and can be found with this article online at http://dx.doi.org/10.1016/j.immuni.2013.06.018.

ACKNOWLEDGMENTS

We thank staff in the WEHI Bioservices facility, V. Dixit for *Ripk3*$^{-/-}$ mice, J. Rickard for generating *Ripk3*$^{-/-}$ MDFs, P. Colman and D. Huang for discussions, MX and SAXS beamline staff at the Australian Synchrotron, the Monash University Protein Production Unit for access to the Corbett RT-PCR instrument, and J. Corbin, L. DiRago, C. Hyland, S. Mifsud, D. Stockwell, and T. Willson for technical assistance. This work was supported by NHMRC grants (1016647, 461221, 1016701, 637342, 1025594, 1046984) and fellowships to J.M.H., I.J.M., D.J.H., N.A.N., A.S., J.S., and W.S.A.; ARC fellowships to J.M.M., P.E.C., T.O., and J.J.B.; a Cancer Council Victoria fellowship to D.M.; Leukaemia Foundation and Australian Stem Cell Centre scholarships to L.N.V.; and additional support from the Australian Cancer Research Fund, Victorian State Government Operational Infrastructure Support, and NHMRC IRIISS grant (361646).

Received: November 20, 2012
Accepted: June 20, 2013
Published: September 5, 2013

REFERENCES

Adams, P.D., Afonine, P.V., Bunkóczi, G., Chen, V.B., Davis, I.W., Echols, N., Headd, J.J., Hung, L.W., Kapral, G.J., Grosse-Kunstleve, R.W., et al. (2010). PHENIX: a comprehensive Python-based system for macromolecular structure solution. Acta Crystallogr. D Biol. Crystallogr. *66*, 213–221.

Alexander, W.S., Roberts, A.W., Nicola, N.A., Li, R., and Metcalf, D. (1996). Deficiencies in progenitor cells of multiple hematopoietic lineages and defective megakaryocytopoiesis in mice lacking the thrombopoietic receptor c-Mpl. Blood *87*, 2162–2170.

Bossen, C., Ingold, K., Tardivel, A., Bodmer, J.L., Gaide, O., Hertig, S., Ambrose, C., Tschopp, J., and Schneider, P. (2006). Interactions of tumor necrosis factor (TNF) and TNF receptor family members in the mouse and human. J. Biol. Chem. *281*, 13964–13971.

Boudeau, J., Miranda-Saavedra, D., Barton, G.J., and Alessi, D.R. (2006). Emerging roles of pseudokinases. Trends Cell Biol. *16*, 443–452.

Carrera, A.C., Alexandrov, K., and Roberts, T.M. (1993). The conserved lysine of the catalytic domain of protein kinases is actively involved in the phosphotransfer reaction and not required for anchoring ATP. Proc. Natl. Acad. Sci. USA *90*, 442–446.

Cho, Y.S., Challa, S., Moquin, D., Genga, R., Ray, T.D., Guildford, M., and Chan, F.K. (2009). Phosphorylation-driven assembly of the RIP1-RIP3 complex regulates programmed necrosis and virus-induced inflammation. Cell *137*, 1112–1123.

Cronin, C.N., Lim, K.B., and Rogers, J. (2007). Production of selenomethionyl-derivatized proteins in baculovirus-infected insect cells. Protein Sci. *16*, 2023–2029.

Degterev, A., Huang, Z., Boyce, M., Li, Y., Jagtap, P., Mizushima, N., Cuny, G.D., Mitchison, T.J., Moskowitz, M.A., and Yuan, J. (2005). Chemical inhibitor of nonapoptotic cell death with therapeutic potential for ischemic brain injury. Nat. Chem. Biol. *1*, 112–119.

Duprez, L., Takahashi, N., Van Hauwermeiren, F., Vandendriessche, B., Goossens, V., Vanden Berghe, T., Declercq, W., Libert, C., Cauwels, A., and Vandenabeele, P. (2011). RIP kinase-dependent necrosis drives lethal systemic inflammatory response syndrome. Immunity *35*, 908–918.

Emsley, P., Lohkamp, B., Scott, W.G., and Cowtan, K. (2010). Features and development of Coot. Acta Crystallogr. D Biol. Crystallogr. *66*, 486–501.

Eyers, P.A., and Murphy, J.M. (2013). Dawn of the dead: protein pseudokinases signal new adventures in cell biology. Biochem. Soc. Trans. *41*, 969–974.

Forbes, S.A., Bhamra, G., Bamford, S., Dawson, E., Kok, C., Clements, J., Menzies, A., Teague, J.W., Futreal, P.A., and Stratton, M.R. (2008). The Catalogue of Somatic Mutations in Cancer (COSMIC). Curr. Protoc. Hum. Genet. *Chapter 10*, Unit 10.11.

Hanks, S.K., Quinn, A.M., and Hunter, T. (1988). The protein kinase family: conserved features and deduced phylogeny of the catalytic domains. Science *241*, 42–52.

He, S., Wang, L., Miao, L., Wang, T., Du, F., Zhao, L., and Wang, X. (2009). Receptor interacting protein kinase-3 determines cellular necrotic response to TNF-alpha. Cell *137*, 1100–1111.

Huse, M., and Kuriyan, J. (2002). The conformational plasticity of protein kinases. Cell *109*, 275–282.

Jaleel, M., Saha, S., Shenoy, A.R., and Visweswariah, S.S. (2006). The kinase homology domain of receptor guanylyl cyclase C: ATP binding and identification of an adenine nucleotide sensitive site. Biochemistry *45*, 1888–1898.

Kang, T.B., Yang, S.H., Toth, B., Kovalenko, A., and Wallach, D. (2013). Caspase-8 blocks kinase RIPK3-mediated activation of the NLRP3 inflammasome. Immunity *38*, 27–40.

Langer, G., Cohen, S.X., Lamzin, V.S., and Perrakis, A. (2008). Automated macromolecular model building for X-ray crystallography using ARP/wARP version 7. Nat. Protoc. *3*, 1171–1179.

Lo, M.C., Aulabaugh, A., Jin, G., Cowling, R., Bard, J., Malamas, M., and Ellestad, G. (2004). Evaluation of fluorescence-based thermal shift assays for hit identification in drug discovery. Anal. Biochem. *332*, 153–159.

Lucet, I.S., Babon, J.J., and Murphy, J.M. (2013). Techniques to examine nucleotide binding by pseudokinases. Biochem. Soc. Trans. *41*, 975–980.

Manning, G., Whyte, D.B., Martinez, R., Hunter, T., and Sudarsanam, S. (2002). The protein kinase complement of the human genome. Science *298*, 1912–1934.

Micheau, O., Lens, S., Gaide, O., Alevizopoulos, K., and Tschopp, J. (2001). NF-kappaB signals induce the expression of c-FLIP. Mol. Cell. Biol. *21*, 5299–5305.

Murshudov, G.N., Skubák, P., Lebedev, A.A., Pannu, N.S., Steiner, R.A., Nicholls, R.A., Winn, M.D., Long, F., and Vagin, A.A. (2011). REFMAC5 for the refinement of macromolecular crystal structures. Acta Crystallogr. D Biol. Crystallogr. *67*, 355–367.

Newton, K., Sun, X., and Dixit, V.M. (2004). Kinase RIP3 is dispensable for normal NF-kappa Bs, signaling by the B-cell and T-cell receptors, tumor necrosis factor receptor 1, and Toll-like receptors 2 and 4. Mol. Cell. Biol. *24*, 1464–1469.

Otwinowski, Z., and Minor, W. (1997). Processing of X-ray diffraction data collected in oscillation mode. Methods Enzymol. *276*, 307–326.

Saharinen, P., and Silvennoinen, O. (2002). The pseudokinase domain is required for suppression of basal activity of Jak2 and Jak3 tyrosine kinases and for cytokine-inducible activation of signal transduction. J. Biol. Chem. *277*, 47954–47963.

Schwenk, F., Baron, U., and Rajewsky, K. (1995). A cre-transgenic mouse strain for the ubiquitous deletion of loxP-flanked gene segments including deletion in germ cells. Nucleic Acids Res. *23*, 5080–5081.

Shi, F., Telesco, S.E., Liu, Y., Radhakrishnan, R., and Lemmon, M.A. (2010). ErbB3/HER3 intracellular domain is competent to bind ATP and catalyze autophosphorylation. Proc. Natl. Acad. Sci. USA *107*, 7692–7697.

Stachura, D.L., Chou, S.T., and Weiss, M.J. (2006). Early block to erythromegakaryocytic development conferred by loss of transcription factor GATA-1. Blood *107*, 87–97.

Sun, L., Wang, H., Wang, Z., He, S., Chen, S., Liao, D., Wang, L., Yan, J., Liu, W., Lei, X., and Wang, X. (2012). Mixed lineage kinase domain-like protein mediates necrosis signaling downstream of RIP3 kinase. Cell *148*, 213–227.

Taylor, S.S., Keshwani, M.M., Steichen, J.M., and Kornev, A.P. (2012). Evolution of the eukaryotic protein kinases as dynamic molecular switches. Philos. Trans. R. Soc. Lond. B Biol. Sci. *367*, 2517–2528.

Ungureanu, D., Wu, J., Pekkala, T., Niranjan, Y., Young, C., Jensen, O.N., Xu, C.F., Neubert, T.A., Skoda, R.C., Hubbard, S.R., and Silvennoinen, O. (2011). The pseudokinase domain of JAK2 is a dual-specificity protein kinase that negatively regulates cytokine signaling. Nat. Struct. Mol. Biol. *18*, 971–976.

Vandenabeele, P., Galluzzi, L., Vanden Berghe, T., and Kroemer, G. (2010). Molecular mechanisms of necroptosis: an ordered cellular explosion. Nat. Rev. Mol. Cell Biol. *11*, 700–714.

Vanlangenakker, N., Vanden Berghe, T., and Vandenabeele, P. (2012). Many stimuli pull the necrotic trigger, an overview. Cell Death Differ. *19*, 75–86.

Vince, J.E., Wong, W.W., Khan, N., Feltham, R., Chau, D., Ahmed, A.U., Benetatos, C.A., Chunduru, S.K., Condon, S.M., McKinlay, M., et al. (2007). IAP antagonists target cIAP1 to induce TNFalpha-dependent apoptosis. Cell *131*, 682–693.

Vonrhein, C., Blanc, E., Roversi, P., and Bricogne, G. (2007). Automated structure solution with autoSHARP. Methods Mol. Biol. *364*, 215–230.

Wang, Z., Jiang, H., Chen, S., Du, F., and Wang, X. (2012). The mitochondrial phosphatase PGAM5 functions at the convergence point of multiple necrotic death pathways. Cell *148*, 228–243.

Wertz, I.E., and Dixit, V.M. (2010). Regulation of death receptor signaling by the ubiquitin system. Cell Death Differ. *17*, 14–24.

Wu, J., Huang, Z., Ren, J., Zhang, Z., He, P., Li, Y., Ma, J., Chen, W., Zhang, Y., Zhou, X., et al. (2013). Mlkl knockout mice demonstrate the indispensable role of Mlkl in necroptosis. Cell Res. *23*, 994–1006.

Zeqiraj, E., and van Aalten, D.M. (2010). Pseudokinases-remnants of evolution or key allosteric regulators? Curr. Opin. Struct. Biol. *20*, 772–781.

Zhao, J., Jitkaew, S., Cai, Z., Choksi, S., Li, Q., Luo, J., and Liu, Z.G. (2012). Mixed lineage kinase domain-like is a key receptor interacting protein 3 downstream component of TNF-induced necrosis. Proc. Natl. Acad. Sci. USA *109*, 5322–5327.

Zheng, J., Trafny, E.A., Knighton, D.R., Xuong, N.H., Taylor, S.S., Ten Eyck, L.F., and Sowadski, J.M. (1993). 2.2 A refined crystal structure of the catalytic subunit of cAMP-dependent protein kinase complexed with MnATP and a peptide inhibitor. Acta Crystallogr. D Biol. Crystallogr. *49*, 362–365.